

Article

Simulation Modeling and Temperature Over-Advance Perception of Mine Hoist System Based on Digital Twin Technology

Xuejun Liang ^{1,2,3} , Juan Wu ^{1,2,3,*} and Kaiyi Ruan ^{1,2,3}

¹ College of Mechanical and Vehicle Engineering, Taiyuan University of Technology, Taiyuan 030024, China; liangxuejun0060@link.tyut.edu.cn (X.L.)

² Shanxi Province Engineer Technology Research Center for Mine Fluid Control, Taiyuan 030024, China

³ National-Local Joint Engineering Laboratory of Mining Fluid Control, Taiyuan 030024, China

* Correspondence: wujuan@tyut.edu.cn

Abstract: The temperature prediction of hoist motor is one of the effective ways to ensure the safe production of mine hoist. Digital twin technology is a technology that combines the physical system of the real world with the digital model of the virtual world. Through digital twin technology, the physical system in the real world can be monitored and simulated in a virtual environment, and the state information of these systems can be monitored in real time. Recurrent neural network is a kind of neural network suitable for processing sequence data, which can automatically extract and learn the feature information in sequential data. To achieve online monitoring and over-advance perception of the temperature of the mine hoist motor, a temperature prediction and advance sensing method based on digital twins and recurrent neural network is proposed. To begin with, a high-fidelity digital twin monitoring system for mine hoists is constructed, enabling the acquisition of real-time temperature data. These temperature data are then fed into a neural network for feature extraction and precise prediction of the motor's state. Subsequently, based on the temperature prediction module in the digital twin hoist monitoring system, a user interface (UI) is developed, and a fully functional digital twin temperature monitoring system is built and experimentally validated. The experimental results demonstrate that the digital twin system effectively monitors the real-time temperature state of the motor during the operation of the mine hoist. Furthermore, the integration of digital twin and recurrent neural network enables the accurate prediction and proactive detection of temperature variations in the motor of the mine hoist. This innovative approach introduces a novel perspective for implementing predictive maintenance in the mining industry, enhancing the safety and reliability of mine hoists. Additionally, it offers valuable technical support in improving maintenance efficiency and reducing associated costs.

Keywords: mine hoist; digital twin; recurrent neural network; state prediction



Citation: Liang, X.; Wu, J.; Ruan, K. Simulation Modeling and Temperature Over-Advance Perception of Mine Hoist System Based on Digital Twin Technology. *Machines* **2023**, *11*, 966. <https://doi.org/10.3390/machines11100966>

Academic Editors: Hongli Gao and Zhichao You

Received: 19 September 2023

Revised: 6 October 2023

Accepted: 13 October 2023

Published: 17 October 2023



Copyright: © 2023 by the authors. Licensee MDPI, Basel, Switzerland. This article is an open access article distributed under the terms and conditions of the Creative Commons Attribution (CC BY) license (<https://creativecommons.org/licenses/by/4.0/>).

1. Introduction

As a crucial component of the coal mine infrastructure, ensuring the safe and stable operation of the mine hoist is of utmost importance for maintaining the overall productivity of the mine [1]. During motor operation, there is a high likelihood of overheating, which poses a significant risk. Prolonged overheating can lead to motor winding damage, resulting in severe consequences such as complete failure of the hoist's traction system and irreparable and catastrophic accidents [2].

Extensive research has been conducted by scholars on the monitoring and estimation of motor temperature. Jiang Shuanlei et al. [3] developed an online motor temperature monitoring system that utilizes LoRa wireless communication and virtual instruments. Popov, N.Z. et al. [4] introduced a novel sensorless temperature estimator for permanent magnet synchronous motor drivers. Yutthanawa, A. et al. [5] used an automatic machine

learning method to estimate the temperature of a multi-surface permanent magnet synchronous motor. Kirchgassner, W. et al. [6] employed deep loops and convolutional neural networks with residual connections to predict high dynamic temperatures within permanent magnet synchronous motors, eliminating the need for domain expertise or specific drive chain specifications in topology design.

Digital twin, a novel technology capable of capturing the entire life cycle process of the corresponding physical equipment [7,8], has been recognized as a disruptive technology and one of the top ten strategic science and technology trends by Goldner [9,10]. Currently, digital twin technology has undergone broad research and application in sectors such as healthcare [11,12], electric power [13,14], and smart cities [15]. In contrast, the implementation of digital twins in the mining industry has been relatively recent but holds significant potential with a wide range of application scenarios. In previous studies, Kalinowski, P. et al. [16] suggested employing a combination of digital 3D structure models, BIM, and digital twins for diagnosing and monitoring the infrastructure of shaft hoisting systems. Jacobs, D.R. et al. [17] utilized digital twins to simulate and plan comprehensive ventilation networks in deep mines, enabling the identification and diagnosis of high-risk areas prone to high temperatures, dust absorption, and gas accumulation. Additionally, digital twins have been applied to monitor the temperature of electric motors. Li Heng et al. [18] proposed a thermal sensing digital twin model based on BP neural networks to precisely estimate motor torque and speed. Venkatesan, S. et al. [19] developed intelligent digital twins in MATLAB/Simulink for health condition monitoring, including temperature, and established a remote monitoring center. Brandtstaedter, H. et al. [20] presented the application of digital twins in large electric drive trains. Their model-based simulation approach enables monitoring and prediction of the system behavior, including the temperature of the synchronous motor during power-on scenarios.

In this paper, the monitoring data are obtained through the intelligent sensing sensor network of mine hoist, the digital twin model of physical entity object is established, and the digital twin system of mine hoist is constructed. The main objective of this paper is to analyze the prediction of temperature and the perception of over-advance in the mine hoist motor using a fusion method that combines the digital twin model with neural networks. The real-time temperature data from multiple points on the hoist motor are acquired and preprocessed. Subsequently, the data are fed into the neural network individually, and the optimal model is determined through comparative training. This enables the prediction of temperature data for each cycle of the lifting process, thereby facilitating the over-advance perception of motor temperature.

2. Construction of a Digital Twin Monitoring System for Mine Hoists

2.1. Composition of the Monitoring System

The mine hoist monitoring system based on digital twin technology encompasses five dimensions: virtual digitization, simulation interaction, online perception, over-perception, and twin co-intelligence, as shown in Figure 1. In the process of operation, the system continuously learns, grows, and improves its functions required for practical production. The whole system is not only driven by the real world, but in turn leads the changes within it. This paper focus on analyzing the dynamic prediction of motor temperature, which surpasses the conventional real-time tracking. Temperature over-advance perception is no longer satisfied with the real-time dynamic following of the motor temperature, it also involves predicting the temperature dynamics based on the analysis of real-time data acquisition and its underlying mechanisms.

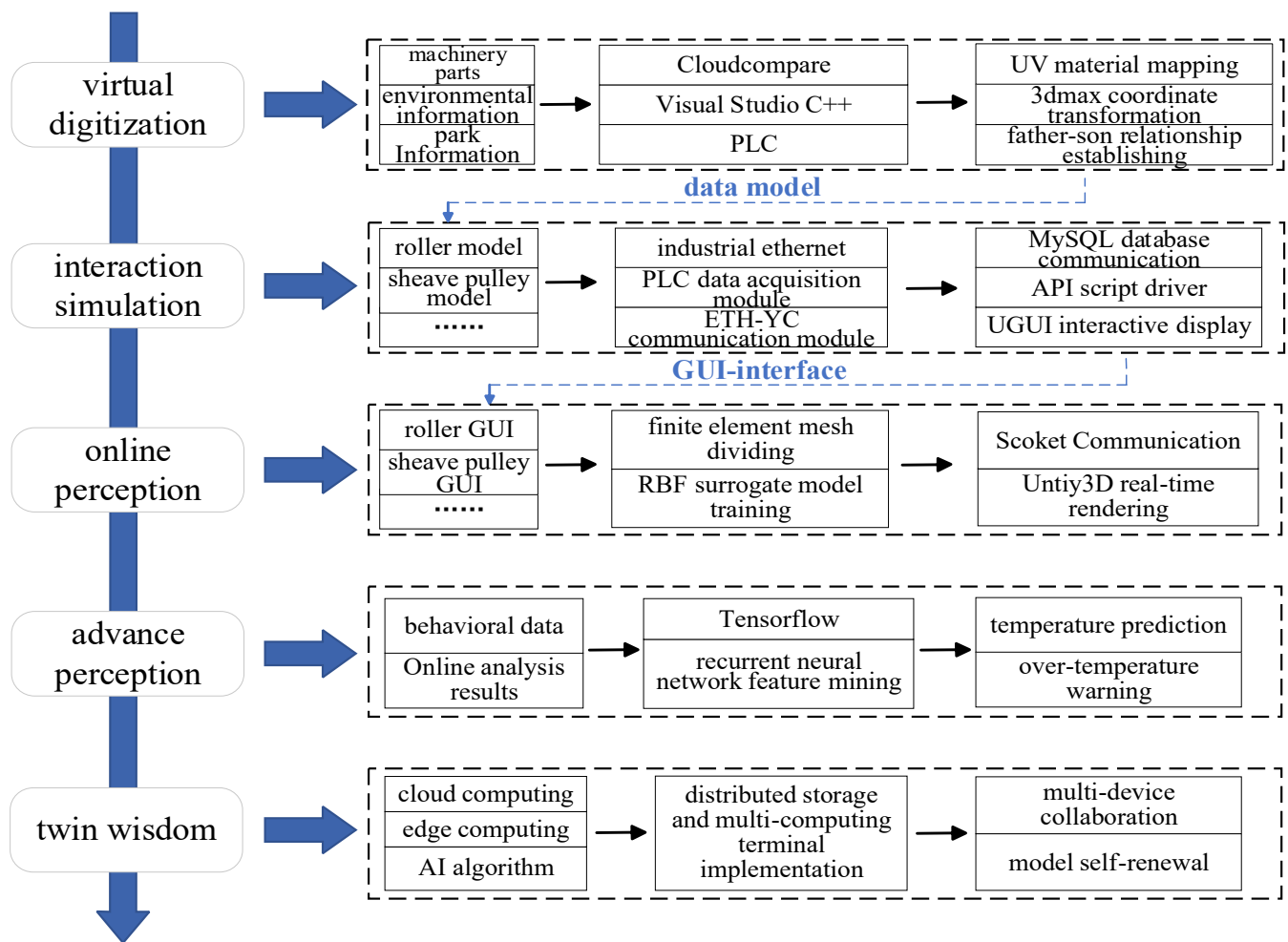


Figure 1. Digital twin five-dimensional maturity model of mine hoist.

2.2. Construction of the Monitoring System

Given the large scale and numerous components of the mine hoisting system, a 3D laser point cloud-based geometric modeling method was employed. The 3D point cloud data of the mine shaft are obtained by scanning the entire mine hoist using a handheld 3D laser scanner (GeoSLAM system). During the scanning of the point cloud data, a specific path scanning optimization scheme is implemented to maximize the preservation of point cloud integrity and accelerate data acquisition speed. Various parameters are configured to apply radius and statistical joint filtering to the point cloud, aiming to identify the optimal combination of filtering parameters. Then, poisson surface reconstruction is carried out on the processed point cloud data of the mine hoisting system to generate a realistic three-dimensional surface model. According to the above point cloud processing, reconstruction, and rendering process for the main shaft and other environmental data, a highly realistic digital twin geometric model of the hoisting machine is finally obtained. The construction of the localized monitoring scene based on digital twin is shown in Figure 2.

Then, based on the reference of the five-dimensional architecture of the digital twin [21], a highly realistic digital twin system for the mine hoist is constructed. This system is capable of simulating the appearance of the hoist and continuously evolving in parallel with the real hoist. This digital twin system possesses the ability to carry out independent learning and exhibit intelligence. The architecture of the system is depicted in Figure 3.

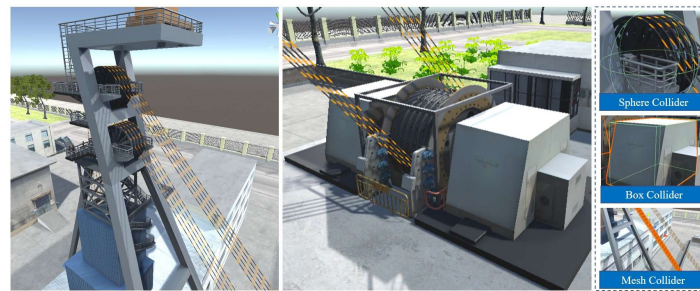


Figure 2. The construction of localized monitoring scene based on digital twin.

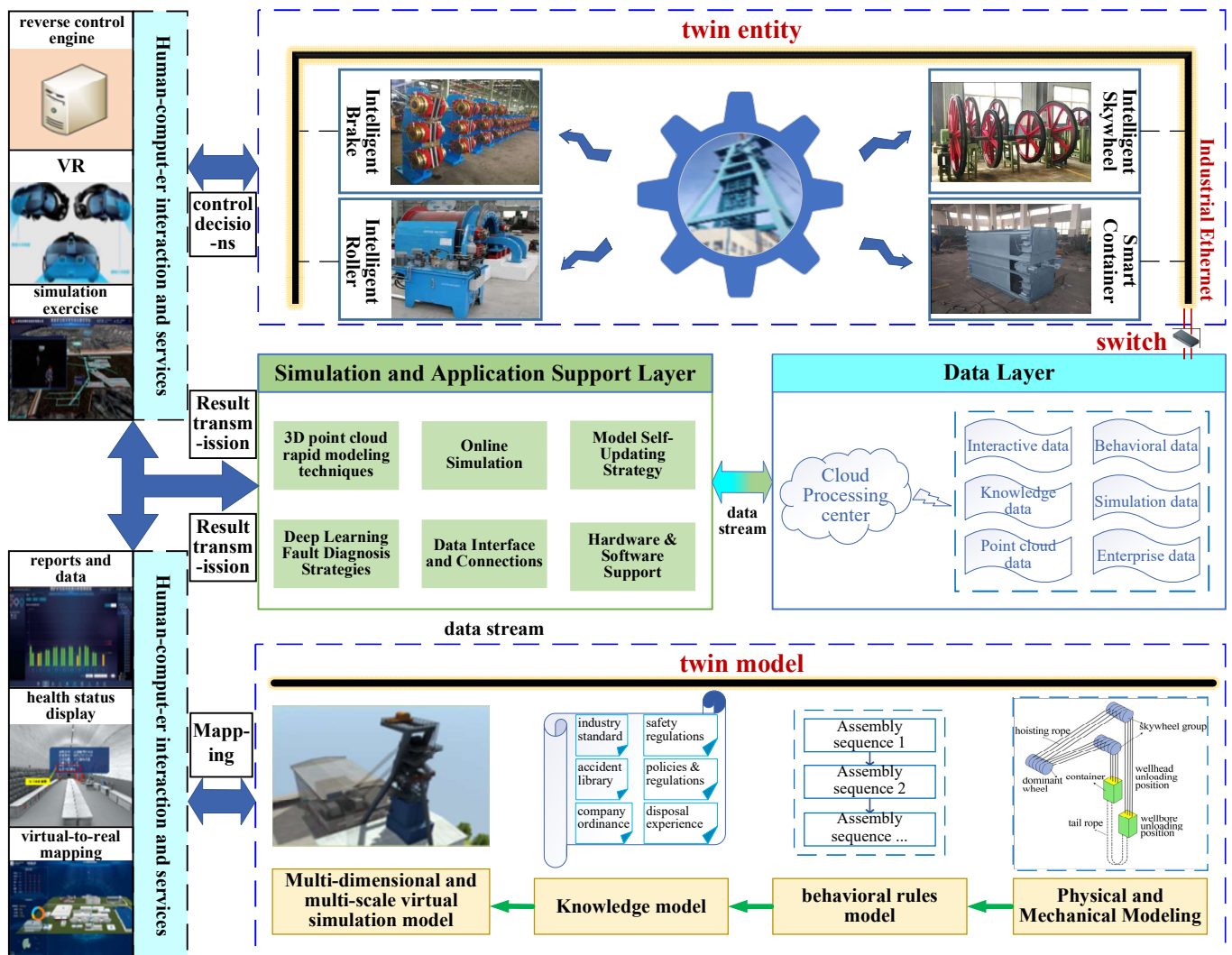


Figure 3. Digital twins structure of mine hoist.

The mine hoist is already equipped with a comprehensive sensing system. Therefore, a behavioral modeling method is proposed, as shown in Figure 4, which makes full use of the existing sensing perceptual network of the mine hoist and the centralized control provided by the Programmable Logic Controller (PLC). This method aims to establish a mapping of the behavioral dimensions within the digital twin, ensuring that the twin exhibits consistent behavior with the physical model over time.

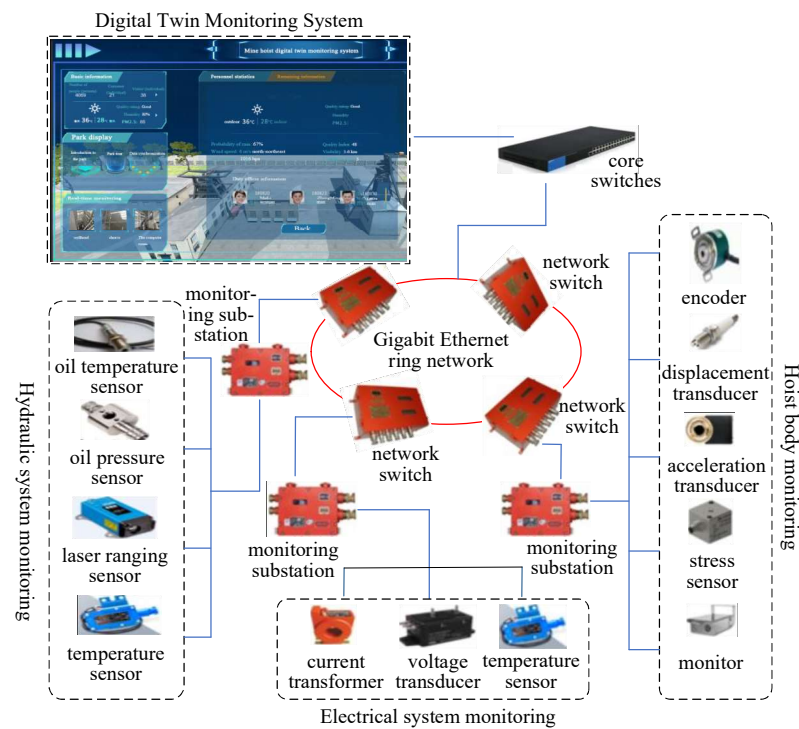


Figure 4. The intelligent sensing network of mine hoist.

3. Twin-Based Data-Driven Over-Advance Sensing of Hoist Motor Temperature

3.1. An RNN-Based Temperature Prediction Method for Hoist Motor

The recurrent neural network (RNN) is a widely used learning model for modeling sequential data. It falls under the category of feedback neural networks and was originally applied in the domain of natural language processing, including tasks like speech recognition and translation [22]. Based on the recursive structure of shared weights, RNN unfolds input sequential data in the direction of time or event evolution for operation, and its basic structure is shown in Figure 5.

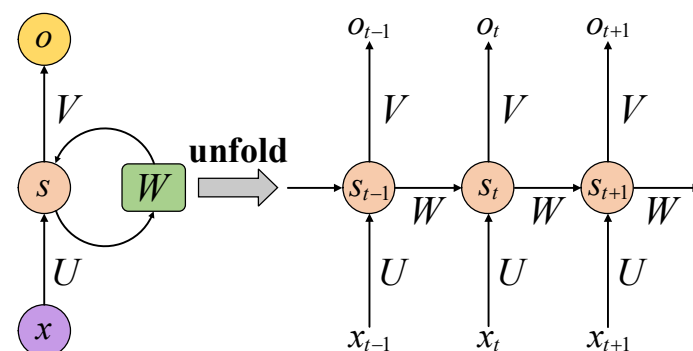


Figure 5. Basic structure diagram of RNN.

In this model, x is the input matrix, U is the weight matrix of the input layer, V is the hidden layer vector, W is the weight matrix of the hidden layer, and o is the output matrix. The hidden layer s_t of the recurrent network at the current time step depends not only on the inputs at the current moment, but also on the hidden layer s_{t-1} from the previous time step. The weight matrix W determines the extent to which information in the hidden layer s_{t-1} is retained. This structure has a natural advantage for processing sequential data as it can dig out relationships between preceding and subsequent sequences and assign weights to form a memory that influences subsequent operations.

3.2. A LSTM-Based Temperature Prediction Method for Hoist Motor

In practical applications, the traditional recurrent neural network (RNN) encounters difficulties in dealing with long-term dependencies and faces challenges such as gradient disappearance or explosion [23]. Consequently, several variants have been developed to address these issues. One notable example is the Long Short-Term Memory (LSTM) network [24]. LSTM incorporates a deliberate design that introduces a “gate” mechanism, analogous to a logic gate, to regulate the flow of information using binary signals of 0 and 1. However, in LSTM, the “gate” mechanism is not simply a binary on or off state, but is controlled by an activation function, which enables the control of the amount of information transmitted.

The main activation functions used in LSTM are sigmoid and tanh, represented by Equations (1) and (2) respectively:

$$\text{sigmoid}(x) = \frac{1}{1 + e^{-x}} \tag{1}$$

$$\text{tanh}(x) = \frac{e^x - e^{-x}}{e^x + e^{-x}} \tag{2}$$

Their function curves are shown in Figure 6:

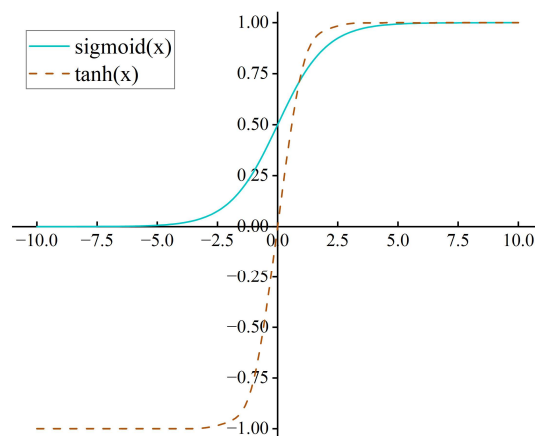


Figure 6. Graph of sigmoid function and tanh function.

According to the graph and formula, it becomes evident that the sigmoid function has a value range of (0, 1). This characteristic limits the output range and enables the mapped matrix to control another matrix through a dot product operation, thereby regulating the amount of information that passes through it. Furthermore, the tanh activation function, which acts in a way that is consistent with the sigmoid function, has a value range of (−1, 1).

The core idea behind LSTM is the introduction of the cell state concept and the ability to make decisions regarding the retention or forgetting of information using the forgetting gate within its memory block. Similar to other recurrent neural networks, LSTM follows a chain-like structure for reusing information, as shown in Figure 7.

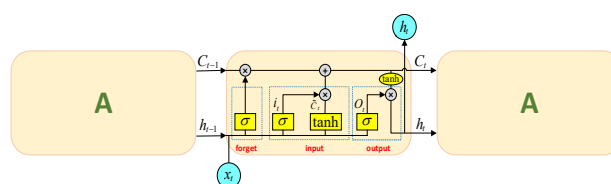


Figure 7. LSTM memory block structure diagram.

The calculation formulas of the input gate, forgetting gate, and internal cell state in LSTM structure are as follows:

$$i_t = \sigma_i(W_i[h_{t-1}, x_t] + b_i) \quad (3)$$

$$f_t = \sigma_f(W_f[h_{t-1}, x_t] + b_f) \quad (4)$$

$$\tilde{C}_t = \tanh(W_c[h_{t-1}, x_t] + b_c) \quad (5)$$

$$C_t = f_t \bullet C_{t-1} + i_t \bullet \tilde{C}_t \quad (6)$$

Among them, σ and \tanh represent the sigmoid and hyperbolic tangent activation functions, respectively, W denotes the corresponding weight matrix, h_{t-1} and x_t refer to the hidden state from the previous time step and the input at the current time step respectively, b represents the corresponding bias matrix, and \bullet signifies the dot product operation.

The above formulas illustrate the roles of various components in the LSTM structure. Specifically, i_t is the input gate, f_t is the forgetting gate, \tilde{C}_t is the internal cell state, C_{t-1} is the cell state in the previous time step, and C_t is the cell state in the current time step. C_t is computed by summing the dot product of f_t and C_{t-1} with the dot product of i_t and \tilde{C}_t . The activation of f_t restricts its value to the range of (0, 1), allowing it to control the amount of information from the previous cell state that contributes to the current operation. This gating mechanism selectively retains information by discarding 0 values and retaining 1 values, playing the role of selection and forgetting. The activation of \tanh limits the value of \tilde{C}_t to the range of (-1, 1), which is advantageous for neural network computations. It is important to note that the computing formulas for i_t and f_t are the same, but they serve different roles. The value of i_t ranges from 0 to 1 and limits the information involved in the calculation, enabling selective retention. These gate operations effectively update C_t to facilitate the calculation of the hidden state.

Then, the output gate and hidden state are calculated. The operation formulas are as follows:

$$o_t = \sigma_o(W_o[h_{t-1}, x_t] + b_o) \quad (7)$$

$$h_t = o_t \bullet \tanh(C_t) \quad (8)$$

Here, o_t represents the output gate, and h_t corresponds to the hidden state at the current time step. Prior to its involvement in the operation, \tanh activation is applied to C_t , which assists in mitigating the problem of gradient explosion and enhances the learning process of neural networks. The activation of o_t is achieved through the sigmoid function, and the value of the cell state C_t is constrained by the dot product operation to obtain h_t .

4. Simulation and Experiment

The digital twin monitoring system incorporates a data over-advance prediction module. This module initially preprocesses the state twin data, which is subsequently fed into the built-in optional neural network (LSTM or RNN) for training. It extracts relevant features and predicts the future state, thereby facilitating over-advance sensing and guiding predictive maintenance. Figure 8 illustrates the specific process of predicting hoist motor temperature based on digital twin data. Four temperature sensors are strategically positioned on the stator winding of the motor, with adjacent sensors spaced 90° apart. The mine hoist intelligent sensing network is employed to monitor the entire lifting process of the mine hoist, capturing real-time temperature data from four motor points (each dataset consists of 1933 consecutive temperature samples). Subsequently, the digital twin monitoring system of the mine hoist is trained in conjunction with a neural network. Through a comparative analysis of the model's prediction output, sensor-measured data, and prediction variances between different networks, the digital twin model and neural network are optimized to enhance the precision of motor temperature prediction. Ultimately, the optimized

prediction model effectively captures the motor temperature trend. The entire process involves a series of successive steps for the twin data. These steps include preprocessing, division of data into training and test sets, normalization, iterative training, selection of the best model, extraction of optimal parameters, anti-normalization, and the utilization of these optimal parameters for predicting the complete motor temperature cycle data, which encompasses loading, unloading, and returning to the bottom of the well. Then, the digital twin monitoring system digitally displays the operating state. Taking advantage of historical state data, the system enables online prediction and advanced perception of the next cycle's state to determine if it exceeds the temperature threshold, thereby providing valuable guidance for predictive maintenance.

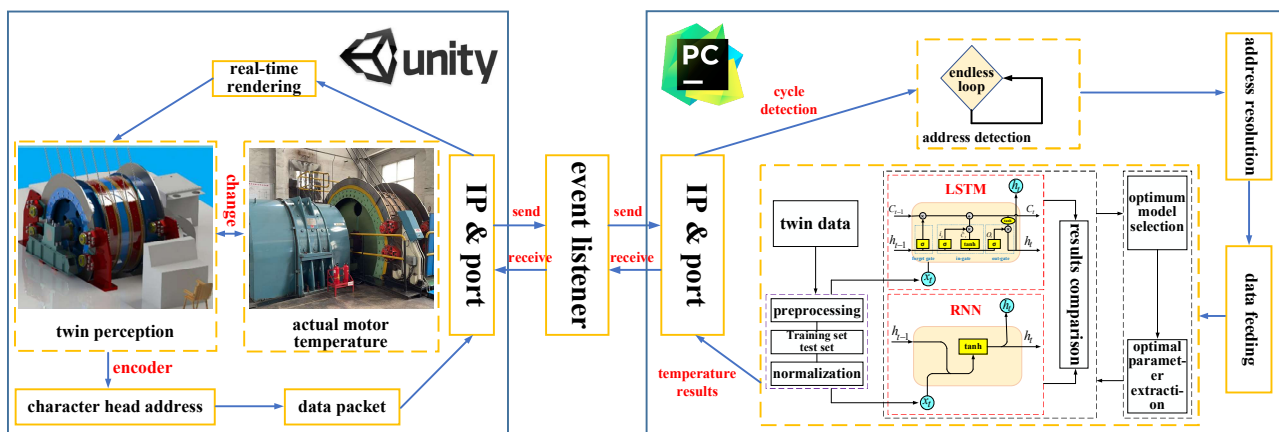


Figure 8. Prediction and sensing flow-chart of hoist based on digital twin.

Motor temperature data exhibit clear time series characteristics, and the influence of past data on future temperature prediction is significant. RNN and LSTM models possess memory functions that allow them to retain historical information, making them suitable for processing sequential data. Previous studies [25,26] have demonstrated the effectiveness of RNN and LSTM models in temperature prediction tasks, validating their feasibility for this purpose. This section constructs RNN and LSTM networks in the neural network prediction section and compares their respective prediction results. For a fair comparison, the network parameters for both LSTM and RNN are kept identical. The RNN and LSTM networks are constructed with two layers of recurrent kernels each, with the first layer having 80 memories and the second layer having 100 memories. A Dropout parameter of 0.2 is employed, and Adam optimization is used. The loss function is defined as the mean square loss. During training, 64 temperature training samples are fed per iteration, with a total of 80 iterations.

4.1. Data Processing

Due to the complex working conditions of the hoist motor, the accuracy of the sensor itself is inherently limited. In addition, noise is introduced during the temperature data acquisition process, which adversely affects the accuracy of the acquired temperature data. Consequently, Gauss–Kalman joint filtering is considered as a method to reduce noise in the acquired data. The data over-prediction module applies Gauss–Kalman joint filtering to the state data in order to mitigate measurement errors caused by sensor limitations and environmental disturbances. The one-dimensional zero-mean Gaussian function for the state data is defined as follows:

$$f(t) = \frac{1}{\sqrt{2\pi}\sigma} e^{-\frac{(t-\mu)^2}{2\sigma^2}} \quad (9)$$

In the above formula, σ is the standard deviation of the Gaussian function, t is the random variable and u is the mean value. As the value of the σ increases, the frequency band of the Gaussian filter widens. This widening results in a broader range of frequencies being considered during the filtering process. Consequently, the filtered data exhibit improved smoothness. In other words, a larger value of the standard deviation enhances the filtering's ability to reduce high-frequency variations, eventually leading to a smoother output.

Kalman filter theory also provides a method to reduce the impact of noise, through the construction of a state space model and the formulation of prediction–update iterative equations for optimal estimation of state variables. The state space equation for the Kalman filter is defined as follows [27]:

$$\begin{cases} x_k = Ax_{k-1} + Bu_{k-1} + w_k \\ z_k = Hx_k + v_k \end{cases} \quad (10)$$

Equation (10) defines the following variables: x_k , z_k , A , B , H , w_k , u_{k-1} , v_k ; they represent the state vector, observation vector, state transfer matrix, input control matrix, observation matrix, process noise vector, system control vector, and measurement noise vector, respectively. It is assumed that w_k and v_k are positive definite, symmetric, uncorrelated, zero-mean Gaussian white noise vectors, and k is a subscript. Then, w_k and v_k fulfill Equation (11):

$$\begin{cases} cov(w_k) = E(w_k w_k^T) = Q \\ cov(v_k) = E(v_k v_k^T) = R \\ E(w_k) = 0, E(v_k) = 0, E(w_k v_k^T) = 0 \end{cases} \quad (11)$$

where cov denotes the covariance, E is the expectation, Q is the covariance matrix of the process noise, and R is the covariance matrix of the observation noise.

The core of the Kalman filter is divided into two main categories: prediction and update. The prediction equation, defined as Equation (12), serves as a fundamental component:

$$\begin{cases} \hat{x}_{\bar{k}} = A\hat{x}_{\bar{k}-1} + Bu_{k-1} \\ P_{\bar{k}} = AP_{\bar{k}-1}A^T + Q \end{cases} \quad (12)$$

The update equation is defined as Equation (13):

$$\begin{cases} K_k = P_{\bar{k}}H^T(HP_{\bar{k}}H^T + R)^{-1} \\ \hat{x}_k = \hat{x}_{\bar{k}} + K_k(z_k - H\hat{x}_{\bar{k}}) \\ P_k = (I - K_kH)P_{\bar{k}} \end{cases} \quad (13)$$

The symbols K_k , \hat{x}_k , P_k , and I in Equations (12) and (13) represent the Kalman gain matrix, the filter optimum, the deviation matrix, and the unit matrix, respectively. By appropriately adjusting the matrices Q and R , the degree of suppression of process noise and measurement noise by the Kalman filter can be controlled and realized. The results obtained from processing a subset of acquired data using the Gauss–Kalman filter are shown in Figure 9.

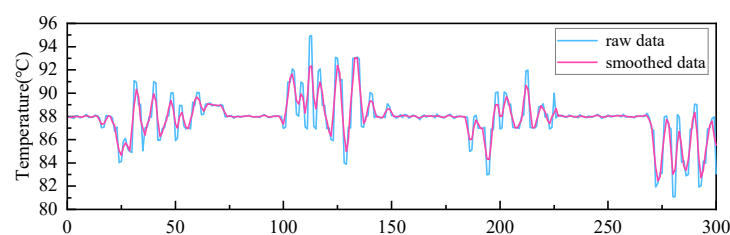


Figure 9. Gauss–Kalman filtering data results.

4.2. Data Training and Evaluation

Considering that the digital twin system undergoes real-time varies, the twin data are consistently fed into the constructed neural network for the purpose of feature extraction. Consequently, this allows for the execution of real-time temperature predictions for the subsequent complete lifting cycle.

For enhanced evaluation and comparison of training results, three metrics are introduced: mean square error (MSE), root mean square error (RMSE), and mean absolute error (MAE). RMSE and MSE are calculated by squaring prediction errors, offering the advantage of considering the variability of errors and being sensitive to large errors or outliers. This is crucial in time series forecasting, as significant errors can have a substantial impact on future predictions. Compared with RMSE and MSE, MAE represents the average absolute value of prediction errors, and it prioritizes the average magnitude of errors rather than their distribution. Unlike RMSE and MSE, MAE is less influenced by outliers and extreme values since it does not involve squaring the errors; these metrics, represented by Equations (14), (15), and (16), respectively, allow for comprehensive comparative assessment.

$$\text{MSE} = \frac{\sum_{i=1}^n (y_i - \hat{y}_i)^2}{n} \quad (14)$$

$$\text{RMSE} = \sqrt{\text{MSE}} \quad (15)$$

$$\text{MAE} = \frac{\sum_{i=1}^n |y_i - \hat{y}_i|}{n} \quad (16)$$

The above equations define the following terms: y_i represents the true value, \hat{y}_i represents the predicted value, n represents the number of predicted samples, MSE represents the mean square error, RMSE represents the root mean square error, and MAE represents the mean absolute error.

The primary objective in temperature prediction is to determine if the maximum temperature exceeds the motor's maximum tolerance limit. Therefore, the accurate prediction of temperature extremes is crucial. However, during the motor's shutdown at low temperatures, the prediction data may exhibit some degree of fluctuation. These characteristics align with the mathematical properties of the evaluation indices trained by the LSTM network. Specifically, when the temperature extreme value prediction is accurate, and the prediction results of other temperature points have errors, the evaluation index values are better than the evaluation index with large temperature extreme value prediction error and good prediction adaptability of other sections. Thus, it is acceptable to choose the above evaluation metrics to measure the excellence of the final results.

4.3. Analysis of Training Results

By analyzing the temperature behavior of the hoist motor, it is found that the temperature change rule of the hoist motor shows cyclic changes that align with the hoisting production behavior. The training set comprises temperature state data from the initial 25 lifting behaviors in a day, which are used to predict the temperature data for the 26th lifting behavior of the hoist motor. The validation set consists of the actual temperature data from the 26th hoisting behavior. The prediction results for the temperature of four sensors are compared. The training and prediction outcomes for temperature point sensor 1 are shown in Figure 10.

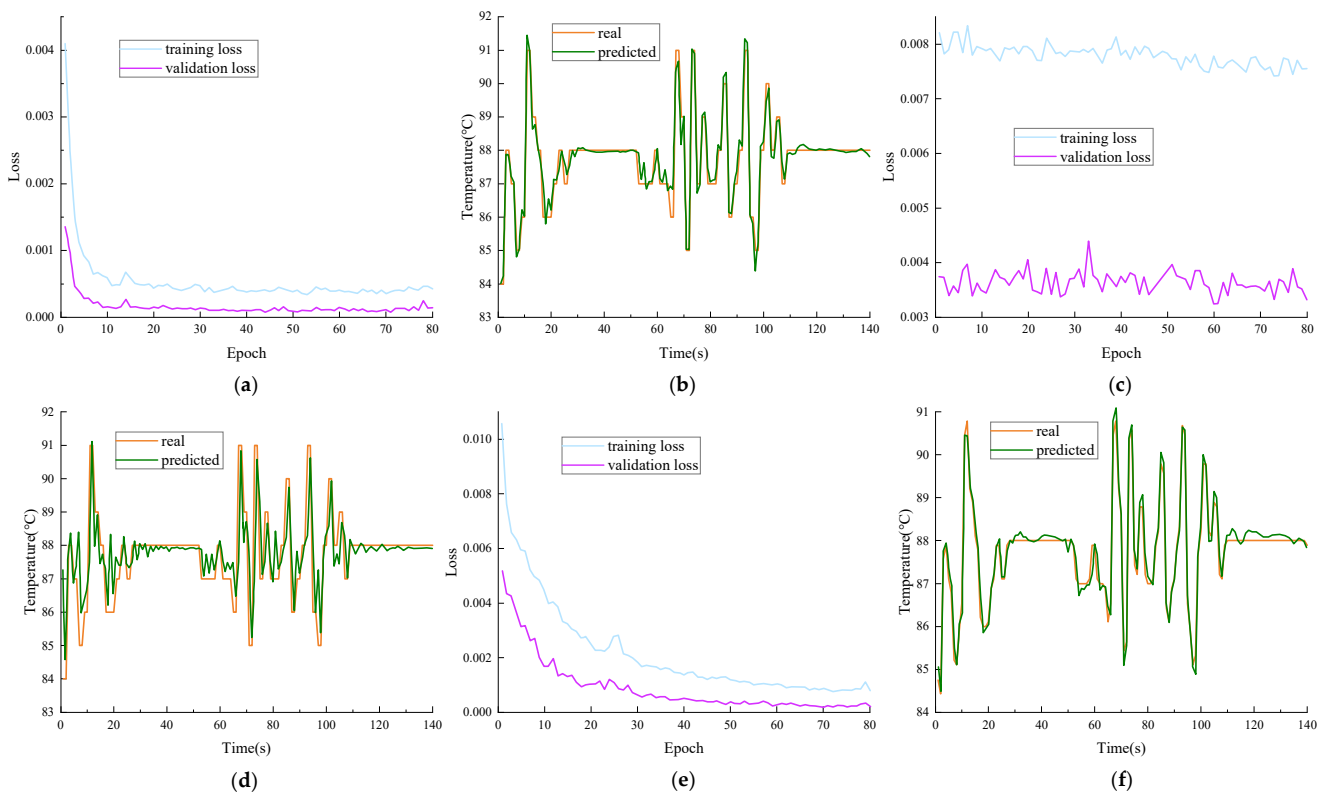


Figure 10. Comparison chart of training and prediction results for temperature point sensor 1: (a) loss of LSTM; (b) prediction of LSTM; (c) loss of RNN; (d) prediction of RNN; (e) loss of Gauss–Kalman–LSTM; (f) prediction of Gauss–Kalman–LSTM.

During the training process, it is evident that the gradient of the RNN network disappears, while the loss function of the LSTM network consistently decreases and stabilizes around the 30th epoch, resulting in superior training outcomes. Upon comparing the prediction results, it becomes evident that the RNN network exhibits significant fluctuations in each section of the lifting motor operation, and its prediction of the highest temperature is inaccurate. Conversely, the LSTM network outperforms the RNN network in terms of prediction accuracy. While the predicted temperature trends and values approximate the actual temperatures for each section, some peak temperature points have inaccurate predictions. The temperature state data, after applying Gauss–Kalman joint filtering, reveal a favorable trend in the loss function and achieve better accuracy in predicting maximum temperatures compared to the LSTM network without filtering. The temperature prediction results were higher than the actual values at many points, with a maximum overestimation of 0.4 °C. This is sufficient to meet the requirements for temperature failure warning in practice, namely, predicted temperatures should be slightly higher than actual values within a reasonable range. This helps reserve time in advance for fault disposal.

In Figure 10, only out-of-sample predictions are displayed. However, based solely on the predicted values, it is not possible to determine whether there is a statistically significant difference between the predictions of the LSTM and Gauss–Kalman–LSTM models. Therefore, we followed a statistical testing method reported in [28] for comparing the predictive accuracy of the two model groups. The results are shown in Figure 11, with a histogram of the error distribution on the left and an empirical cumulative distribution function (CDF) on the far right.

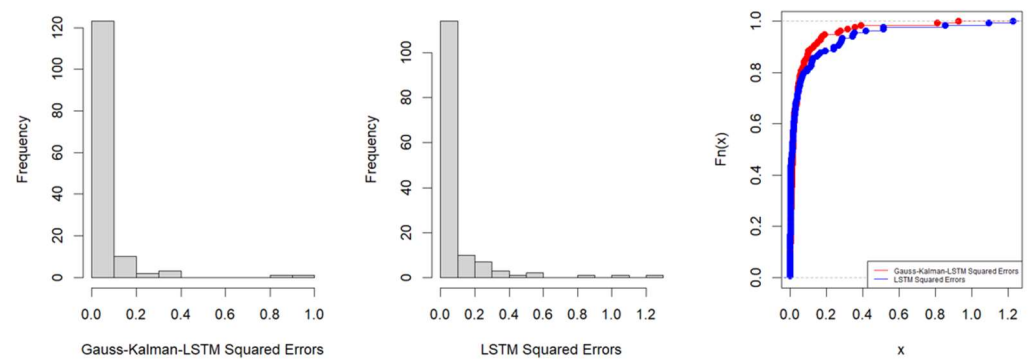


Figure 11. Distribution of errors and empirical CDF of errors.

In this case, we can see that the errors of the Gauss–Kalman–LSTM model are more concentrated within a lower range, while the errors of the other model are more dispersed. Based on this analysis, it can be inferred that there is a significant difference in predictive accuracy between the two models. Additionally, the CDF curve of the Gauss–Kalman–LSTM errors is positioned above the CDF curve of the other group of errors, this observation suggests that the overall distribution of errors for the Gauss–Kalman–LSTM model is smaller, indicating that the corresponding model likely possesses superior predictive accuracy.

A similar process was applied to data from temperature point sensor 2, but the purpose of this set of data is only for predictive comparison, without analyzing significant differences between the models. The results of model training and prediction performance are shown in Figure 12 for comparison.

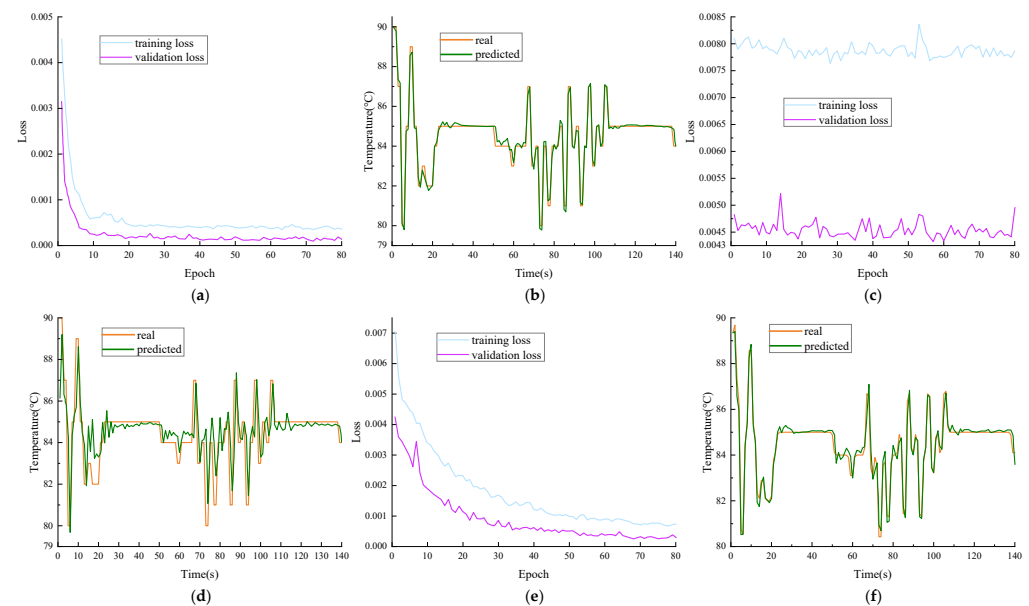


Figure 12. Comparison chart of training and prediction results for temperature point sensor 2: (a) loss of LSTM; (b) prediction of LSTM; (c) loss of RNN; (d) prediction of RNN; (e) loss of Gauss–Kalman–LSTM; (f) prediction of Gauss–Kalman–LSTM.

The training and prediction results for temperature point sensors 1 and 2 are identical. Specifically, the temperature prediction results after applying Gauss–Kalman joint filtering outperform those obtained without neural network filtering. The prediction results of temperature point sensors 3 and 4 also align with the aforementioned conditions. To further compare the prediction results, evaluation metrics are introduced as shown in Table 1.

Table 1. Comparison table of evaluation indexes.

No.	RNN			LSTM			Gauss–Kalman–LSTM		
	MSE	RMSE	MAE	MSE	RMSE	MAE	MSE	RMSE	MAE
1	0.9308	0.9648	0.5308	0.0998	0.3159	0.2138	0.0134	0.1158	0.0790
2	1.3327	1.1544	0.6895	0.0906	0.3010	0.2093	0.0676	0.2600	0.1725
3	1.5396	1.2408	0.6177	0.0627	0.2505	0.1599	0.0405	0.2012	0.1281
4	1.73594	1.3175	0.6903	0.2143	0.4630	0.3091	0.0559	0.2365	0.1643

Through a comparison and analysis of the evaluation indices in Table 1, it is evident that the LSTM network training results with Gauss–Kalman joint filtering exhibit smaller values for MSE, RMSE, and MAE compared to the other two methods. This indicates a higher level of accuracy in predicting the maximum temperature value. Thus, the over-advance prediction module in the digital twin monitoring system reads the twin data, applies the Gauss–Kalman joint filtering process, and then undergoes LSTM network training and prediction. This approach enables the online prediction of the next cycle’s state using historical data, allowing for the determination of whether it will exceed the temperature threshold. This over-advance perception can definitely facilitate in guiding predictive maintenance efforts.

4.4. Experimental Study

Taking the main hoisting system of a specific mine in China as an example, it has a lifting height of 483 m and a lifting capacity of 30 tons. Figure 13 illustrates the operation process of the mine hoisting system. Focusing on the east skip, we can see that it begins by stopping at a depth of approximately 470 m at the bottom of the well for loading. After loading, it accelerates to a constant speed for lifting and then decelerates to reach the unloading platform at the wellhead for unloading. Once unloaded, it returns to the bottom of the well for reloading. Throughout the entire lifting process, the speed remains consistently stable with small fluctuations. In contrast, the behavior of the west skip is precisely opposite to that of the east skip. Figure 14 illustrates the mine hoist digital twin monitoring system, which is capable of executing various functions, including scene display, human–computer interaction, motion synchronization, and condition monitoring. The current and temperature monitoring of the lifting motor is shown in Figure 15.

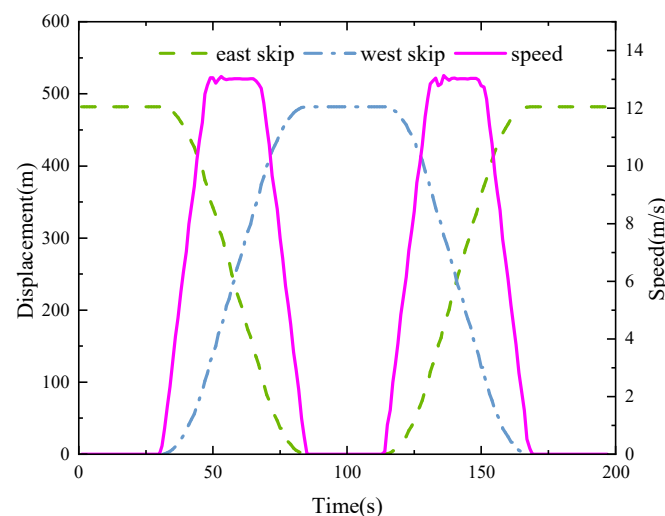
**Figure 13.** Running process diagram of mine hoisting system.



Figure 14. Digital twin monitoring system of mine hoist.

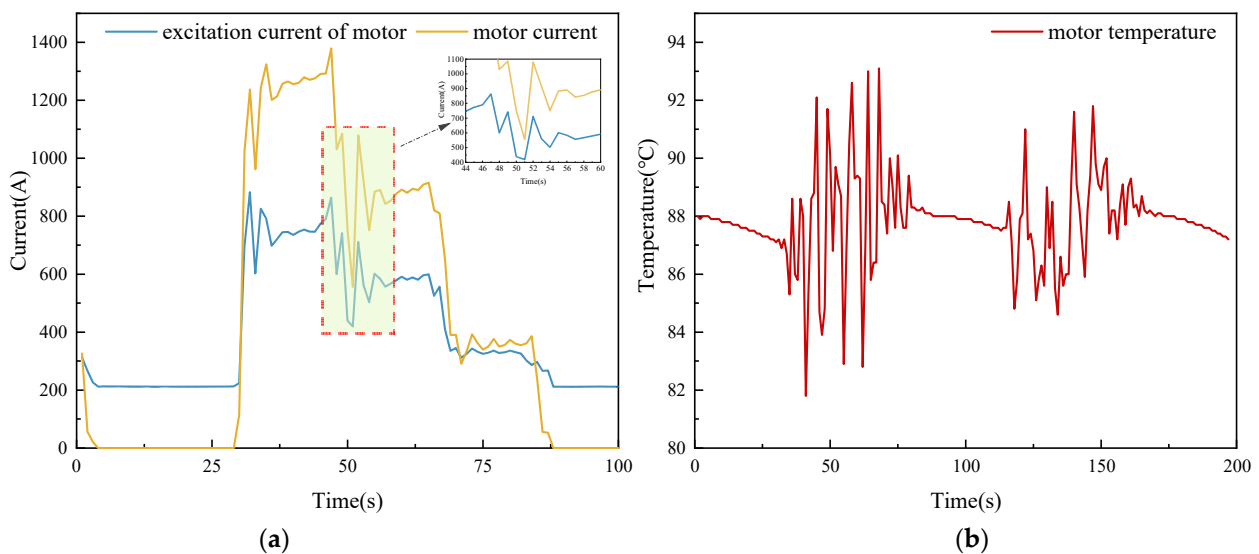


Figure 15. Current and temperature behavioral monitoring of hoist motor: (a) current monitoring; (b) temperature monitoring.

The digital twin monitoring system of the mine hoist incorporates an interface constructed using the temperature prediction module, which graphically displays the prediction results. Simultaneously, the script API is employed to trigger an alarm response when the temperature prediction data exceed the temperature threshold (shown in Figure 16). It can be seen from Figure 16 that the temperature prediction and early warning UI interface of the machine room motor can display essential information such as motor model and rated parameters. Additionally, it can predict the parameters of the motor, motor excitation current, drum speed, and motor temperature for the next lifting cycle during the current hoist operation cycle. During the operation of the mine hoist, if the predicted temperature value for the next motor cycle exceeds the normal temperature threshold, the health status

text content in the basic information panel will indicate that the temperature exceeds the standard. The curve will be highlighted in red, serving as an early warning of a fault, and necessitating the machine to be stopped for maintenance. The fault prediction module effectively evaluates and alerts the health status of the hoist, enabling a monitoring mode based on virtual monitoring supplemented by real monitoring.

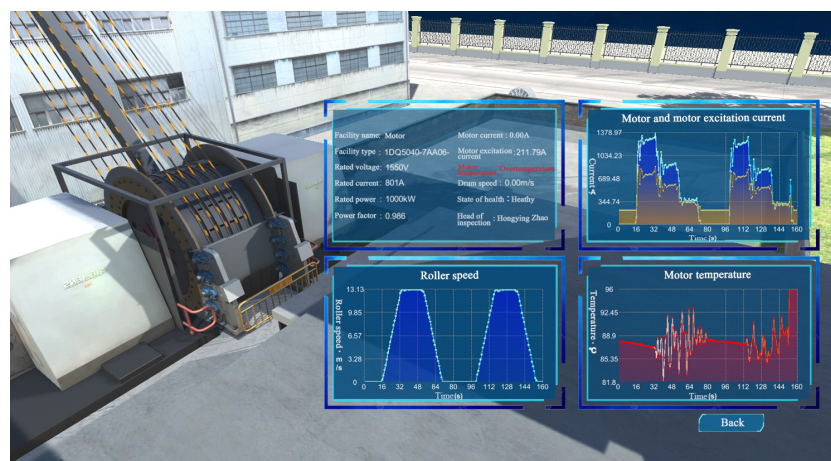


Figure 16. Temperature perception of mine hoist motor in digital twin monitoring system.

5. Conclusions

The mine hoist plays a crucial role in mine production, and its efficient and reliable operation is vital for uninterrupted production and ensuring energy security. This study addresses the issue of mine hoist monitoring by employing the twin fast modeling method to develop a digital twin monitoring system that facilitates multivariate collaborative monitoring. Additionally, deep learning algorithms are utilized to predict the key state variable parameters. The following conclusions have been drawn:

- (1) A five-dimensional framework of mine hoist digital twin is proposed. Each dimension is closely connected through the twin data flow, and the synchronous mapping from the real physical world to the virtual twin world is completed. This framework offers a theoretical support for the development of a mine hoist digital twin system.
- (2) A digital twin state variable prediction module is developed by using the Gauss–Kalman joint filtering algorithm with an LSTM network. This module realizes a more precise prediction of the temperature state data for the hoisting motor, and it presents a new approach to predictive maintenance for the mine hoist. Based on the prediction module, the temperature prediction interface of the hoisting motor is built, which successfully enables motor temperature warnings.

Author Contributions: Writing—original draft preparation, X.L.; writing—review and editing, X.L. and J.W.; conceptualization, K.R. and X.L.; data curation, K.R. and X.L.; funding acquisition, J.W.; project administration, J.W.; supervision, J.W. All authors have read and agreed to the published version of the manuscript.

Funding: This research was funded by the National Natural Science Foundation of China, grant number 52274156.

Institutional Review Board Statement: Not applicable.

Informed Consent Statement: Not applicable.

Data Availability Statement: Not applicable.

Conflicts of Interest: The authors declare no conflict of interest.

References

1. Li, J.; Xie, J.; Yang, Z.; Li, J. Fault Diagnosis Method for a Mine Hoist in the Internet of Things Environment. *Sensors* **2018**, *18*, 1920. [[CrossRef](#)]
2. Sinha, A.K.; Hati, A.S.; Benbouzid, M.; Chakrabarti, P. ANN-Based Pattern Recognition for Induction Motor Broken Rotor Bar Monitoring under Supply Frequency Regulation. *Machines* **2021**, *9*, 87. [[CrossRef](#)]
3. Jiang, S.; Cheng, W.-M. Motor temperature based on LoRa and virtual instrument Online monitoring system research. In Proceedings of the 2019 3rd International Conference on Electronic Information Technology and Computer Engineering (EITCE), Xiamen, China, 18–20 October 2019; pp. 398–401.
4. Popov, N.Z.; Vukosavic, S.N.; Levi, E. Motor Temperature Monitoring Based on Impedance Estimation at PWM Frequencies. *IEEE Trans. Energy Convers.* **2014**, *29*, 215–223. [[CrossRef](#)]
5. Yutthanawa, A.; Wanthong, S.; Inthakheeree, K.; San-Um, W. Multi-surface Permanent Magnet Synchronous Motor Temperature Estimation based on Automate Machine Learning Approach. In Proceedings of the 2023 8th International Conference on Business and Industrial Research (ICBIR), Bangkok, Thailand, 18–19 May 2023; pp. 1051–1055.
6. Kirchgässner, W.; Wallscheid, O.; Böcker, J. Estimating Electric Motor Temperatures with Deep Residual Machine Learning. *IEEE Trans. Power Electron.* **2021**, *36*, 7480–7488. [[CrossRef](#)]
7. Bazi, N.E.; Mabrouki, M.; Laayati, O.; Ouhabi, N.; Hadraoui, H.E.; Hammouch, F.-E.; Chebak, A. Generic Multi-Layered Digital-Twin-Framework-Enabled Asset Lifecycle Management for the Sustainable Mining Industry. *Sustainability* **2023**, *15*, 3470. [[CrossRef](#)]
8. Macchi, M.; Roda, I.; Negri, E.; Fumagalli, L. Exploring the role of digital twin for asset lifecycle management. *IFAC-PapersOnLine* **2018**, *51*, 790–795. [[CrossRef](#)]
9. Brenner, B.; Hummel, V. Digital Twin as Enabler for an Innovative Digital Shopfloor Management System in the ESB Logistics Learning Factory at Reutlingen-University. *Procedia Manuf.* **2017**, *9*, 198–205. [[CrossRef](#)]
10. Uhlemann, T.H.-J.; Schock, C.; Lehmann, C.; Freiburger, S.; Steinhilper, R. The Digital Twin: Demonstrating the Potential of Real Time Data Acquisition in Production Systems. *Procedia Manuf.* **2017**, *9*, 113–120. [[CrossRef](#)]
11. Liu, Y.; Zhang, L.; Yang, Y.; Zhou, L.; Ren, L.; Wang, F.; Liu, R.; Pang, Z.; Jamal, D.M. A Novel Cloud-Based Framework for the Elderly Healthcare Services Using Digital Twin. *IEEE Access* **2019**, *7*, 49088–49101. [[CrossRef](#)]
12. Neghab, H.K.; Jamshidi, M.; Neghab, H.K. Digital Twin of a Magnetic Medical Microrobot with Stochastic Model Predictive Controller Boosted by Machine Learning in Cyber-Physical Healthcare Systems. *Information* **2022**, *13*, 321. [[CrossRef](#)]
13. Fernandes, S.V.; João, D.V.; Cardoso, B.B.; Martins, M.A.I.; Carvalho, E.G. Digital Twin Concept Developing on an Electrical Distribution System—An Application Case. *Energies* **2022**, *15*, 2836. [[CrossRef](#)]
14. Zhou, M.; Yan, J.; Feng, D. Digital twin framework and its application to power grid online analysis. *CSEE J. Power Energy Syst.* **2019**, *5*, 391–398. [[CrossRef](#)]
15. Deng, T.; Zhang, K.; Shen, Z.-J. A systematic review of a digital twin city: A new pattern of urban governance toward smart cities. *J. Manag. Sci. Eng.* **2021**, *6*, 125–134. [[CrossRef](#)]
16. Kalinowski, P.; Długosz, O.; Kamiński, P. *Digital Twin of the Mining Shaft and Hoisting System as an Opportunity to Improve the Management Processes of Shaft Infrastructure Diagnostics and Monitoring*; IntechOpen: London, UK, 2021.
17. Jacobs, D.R.; van Laar, J.H.; Schutte, C.S.L. Strategy to Identify and Mitigate Hazards in Deep-Level Mine Ventilation Systems Using a Calibrated Digital Twin. *S. Afr. J. Ind. Eng.* **2022**, *33*, 204–217. [[CrossRef](#)]
18. Li, H.; Zhu, Z.; He, P.; Yang, Y.; Chen, B.; Peng, J.; Huang, Z. A Thermal-Aware Digital Twin Model of Permanent Magnet Synchronous Motors (PMSM) Based on BP Neural Networks. In Proceedings of the 2022 IEEE International Conference on Trust, Security and Privacy in Computing and Communications (TrustCom), Wuhan, China, 28–30 October 2022; pp. 1099–1106.
19. Venkatesan, S.; Manickavasagam, K.; Tengenkai, N.; Vijayalakshmi, N. Health monitoring and prognosis of electric vehicle motor using intelligent-digital twin. *IET Electr. Power Appl.* **2019**, *13*, 1328–1335. [[CrossRef](#)]
20. Brandtstaedter, H.; Ludwig, C.; Hübner, L.; Tsouchnika, E.; Jungiewicz, A.; Wever, U. Digital Twins for Large Electric Drive Trains. In Proceedings of the 2018 Petroleum and Chemical Industry Conference Europe (PCIC Europe), Antwerpen, Belgium, 5–7 June 2018; pp. 1–5.
21. Wu, C.; Zhou, Y.; Pessôa, M.V.P.; Peng, Q.; Tan, R. Conceptual digital twin modeling based on an integrated five-dimensional framework and TRIZ function model. *J. Manuf. Syst.* **2021**, *58*, 79–93. [[CrossRef](#)]
22. Datta, D.; David, P.E.; Mittal, D.; Jain, A. Neural Machine Translation using Recurrent Neural Network. *Int. J. Eng. Adv. Technol.* **2020**, *9*, 1395–1400. [[CrossRef](#)]
23. Noh, S.-H. Analysis of Gradient Vanishing of RNNs and Performance Comparison. *Information* **2021**, *12*, 442. [[CrossRef](#)]
24. Yang, S.; Yu, X.; Zhou, Y. LSTM and GRU Neural Network Performance Comparison Study: Taking Yelp Review Dataset as an Example. In Proceedings of the 2020 International Workshop on Electronic Communication and Artificial Intelligence (IWECAI), Shanghai, China, 12–14 June 2020; pp. 98–101.
25. Tran, T.T.K.; Bateni, S.M.; Ki, S.J.; Vosoughifar, H. A Review of Neural Networks for Air Temperature Forecasting. *Water* **2021**, *13*, 1294. [[CrossRef](#)]
26. Zhang, W.Y.; Xie, J.F.; Wan, G.C.; Tong, M.S. Single-step and Multi-step Time Series Prediction for Urban Temperature Based on LSTM Model of TensorFlow. In Proceedings of the 2021 Photonics & Electromagnetics Research Symposium (PIERS), Hangzhou, China, 21–25 November 2021; pp. 1531–1535.

27. Khodarahmi, M.; Maihami, V. A Review on Kalman Filter Models. *Arch. Comput. Methods Eng.* **2023**, *30*, 727–747. [[CrossRef](#)]
28. Hassani, H.; Silva, E.S. A Kolmogorov-Smirnov Based Test for Comparing the Predictive Accuracy of Two Sets of Forecasts. *Econometrics* **2015**, *3*, 590–609. [[CrossRef](#)]

Disclaimer/Publisher's Note: The statements, opinions and data contained in all publications are solely those of the individual author(s) and contributor(s) and not of MDPI and/or the editor(s). MDPI and/or the editor(s) disclaim responsibility for any injury to people or property resulting from any ideas, methods, instructions or products referred to in the content.